Supplementary Information for
Molecular basis of human taurine transporter uptake and inhibition

Bowen Du[1#], Lili Cheng[2,3#], Jiaying Xie[1#], Ligong Chen[3]*, Kaige Yan[1,4]*

[1] Shenzhen Key Laboratory of Biomolecular Assembling and Regulation, School of Life Sciences, Southern University of Science and Technology, Shenzhen 518055, China.

[2] Hepatopancreatobiliary Center, Beijing Tsinghua Changgung Hospital, School of Clinical Medicine, Tsinghua Medicine, Tsinghua University, Beijing 102218, China.

[3] State Key Laboratory of Membrane Biology, School of Pharmaceutical Sciences, Key Laboratory of Bioorganic Phosphorus Chemistry and Chemical Biology (Ministry of Education), Tsinghua University, Beijing 100084, China.

[4] Institute for Biological Electron Microscopy, Southern University of Science and Technology, Shenzhen 518055, China.

[#] These authors contributed equally: Bowen Du, Lili Cheng and Jiaying Xie.

* Correspondence:

Ligong Chen: ligongchen@tsinghua.edu.cn;

Kaige Yan: yankg@sustech.edu.cn.

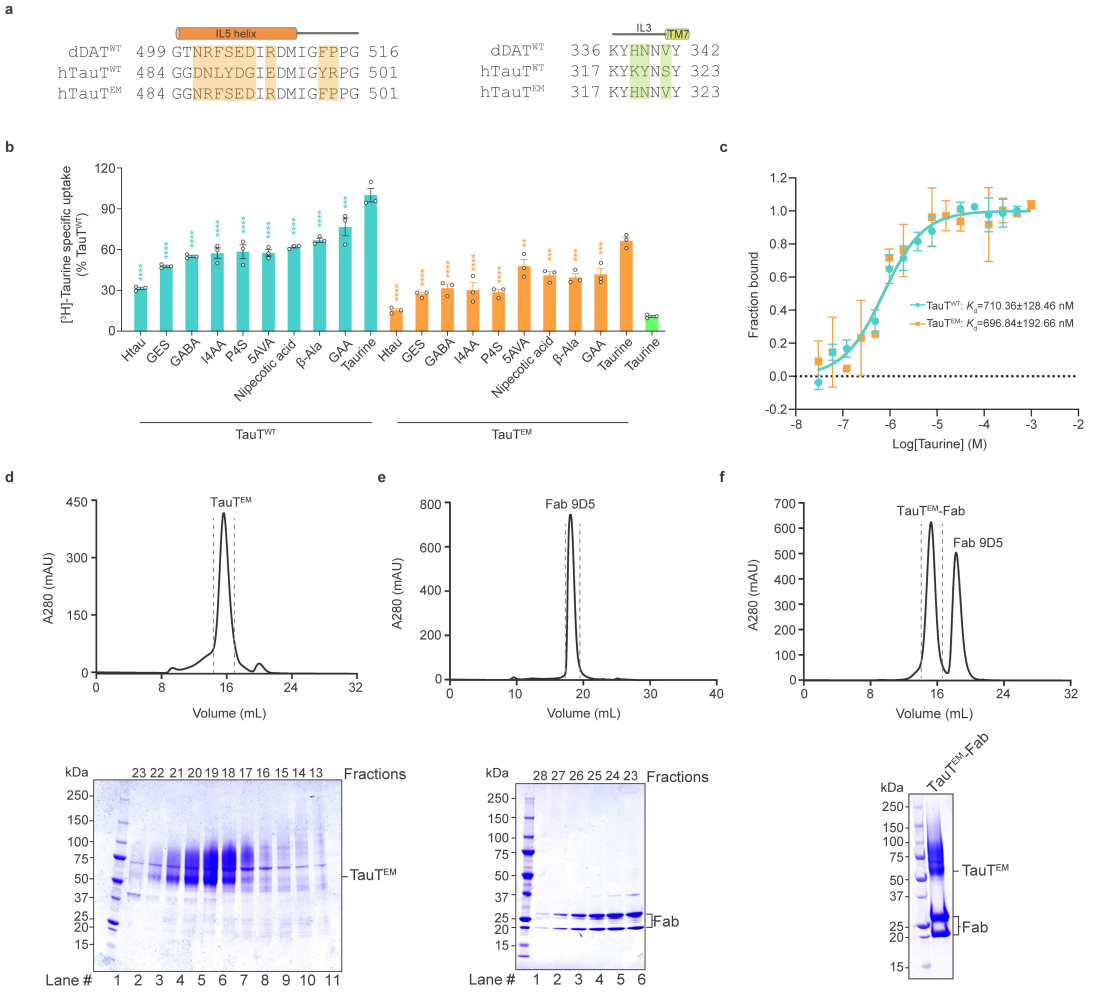

Supplementary Fig. 1 | Functional characterization and purification of hTauT. (a) Sequence alignment of the IL3 and IL5 in dDAT compared with that in hTauT^{WT}. The epitope substitutions made in hTauT^{WT} to prepare the engineered construct, hTauT^{EM}, are highlighted in colored boxes. **(b)** Inhibition of [^{3}H]Taurine-uptake in TauT^{WT} (cyan) and TauT^{EM} (orange). Cells expressing GFP served as control are shown in green. Data were normalized to taurine uptake by TauT^{WT} and are presented as mean ± s.e.m.; n=3 biological replicates. Data were analysed by one-way ANOVA to show the significance compared with TauT^{WT} and TauT^{EM}, respectively: ****P<0.0001, ***P<0.001, **P<0.01. **(c)** Binding affinity for TauT^{WT} and TauT^{EM} with taurine measured using MST assay. Assays were conducted with three independent biological replicates (n=3). Data are mean ± s.e.m. K_d values are presented in nM. Binding curves were plotted by GraphPad Prism. **(d-f)** Protein purification of TauT^{EM} **(d)**, Fab 9D5 **(e)** and cryo-EM sample **(f)**. Peak fractions shown in the top panel were visualized by SDS-PAGE with Coomassie blue staining (below). The excess Fab 9D5 was removed by size-exclusion chromatography on a Superose 6 Increase (10/300) column. Peak fractions used for cryo-EM analysis are indicated by light gray dashed lines. Source data are provided as a Source Data file.

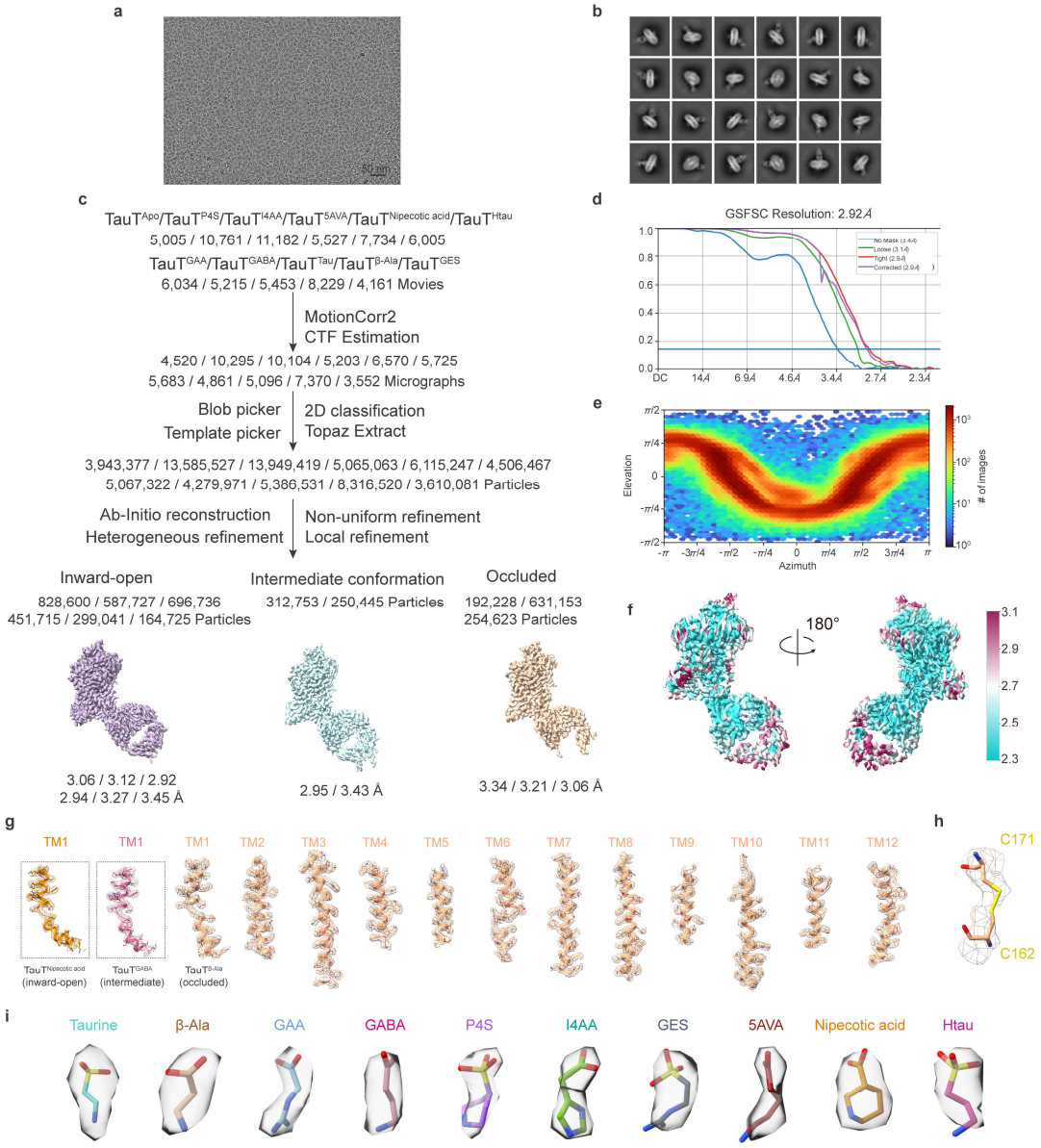

Supplementary Fig. 2 | Data processing of different hTauT datasets and representative cryo-EM densities of TauT structures. (a) Representative motion-corrected cryo-EM micrograph of TauT. **(b)** Representative 2D classes averaged of TauT. **(c)** Flowchart for cryo-EM data processing of $TauT^{Apo}$, $TauT^{P4S}$, $TauT^{I4AA}$, $TauT^{5AVA}$, $TauT^{Nipecotic\ acid}$, $TauT^{Htau}$, $TauT^{GAA}$, $TauT^{GABA}$, $TauT^{Tau}$, $TauT^{β\text{-}Ala}$ and $TauT^{GES}$. The final density maps are contoured at 5.4 σ by ChimeraX. **(d-f)** Using $TauT^{I4AA}$ as an example to show the gold standard Fourier shell correlation (FSC) curve for the 3D refinement **(d)**, angular distribution of the particles used for final reconstitution **(e)** and local resolution distribution of the sharpened maps calculated by cryoSPARC **(f)**. **(g)** Representative cryo-EM densities for the TMs of TauT. The densities are contoured at 4.5 σ by ChimeraX. Cryo-EM density for the TM1 segment of the inward-open $TauT^{Nipecotic\ acid}$ (orange) and $TauT^{GABA}$ (pink) captured in intermediate conformation are also shown. **(h)** Cryo-EM map of the disulfide bond between Cys162 and Cys171 in $TauT^{β\text{-}Ala}$ and EM densities are contoured at 2.6 σ by

ChimeraX. **(i)** Densities of small molecules in the structures of TauT complexes. The densities are contoured at 4.5 σ by ChimeraX.

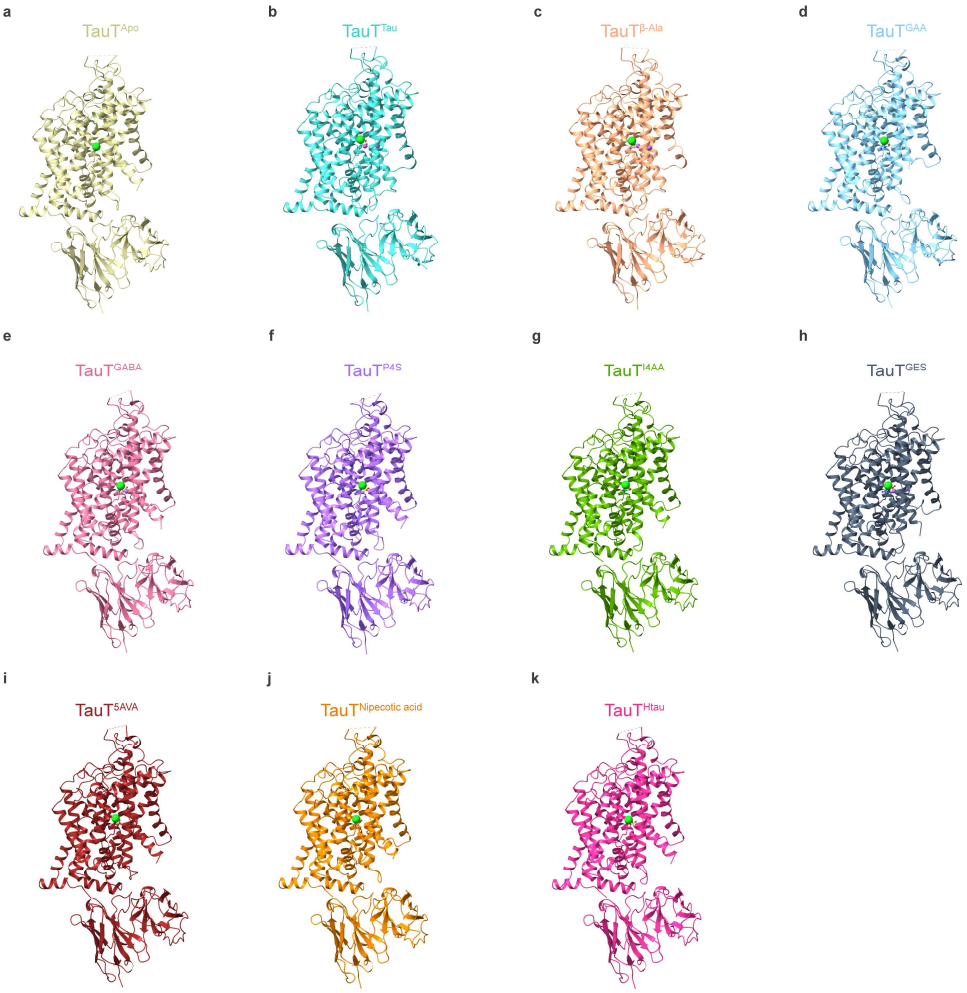

Supplementary Fig. 3 | Cryo-EM structural determination of human TauT in distinct states. Overall structures of apo **(a),** taurine-bound **(b),** beta-alanine-bound **(c),** guanidinoacetate-bound **(d),** gamma-aminobutyric acid-bound **(e),** piperidine-4-sulfonic acid-bound **(f),** imidazole-4-acetatic acid-bound **(g),** guanidinoethyl sulphonate-bound **(h),** 5-aminovaleric acid-bound **(i),** nipecotic acid-bound **(j)** and homotaurine-bound **(k)** TauT interacting with the Fab 9D5. Sodium and chloride ions are shown as purple and green spheres, respectively. Bound ligands are displayed as ball sticks.

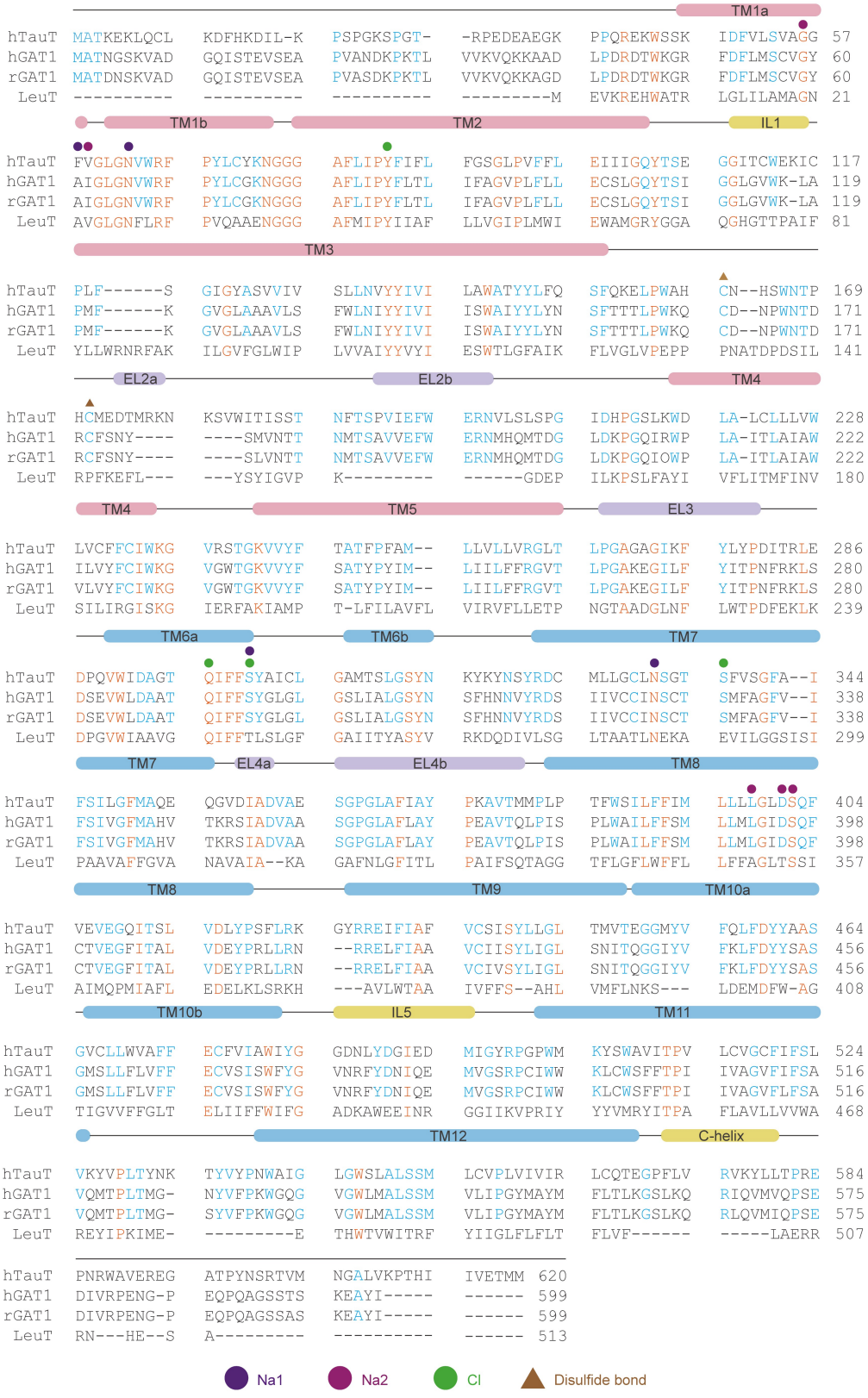

Supplementary Fig. 4 | Sequence alignment of hTauT, hGAT1, rGAT1 and LeuT. TM, IL and EL of hTauT are indicated above the alignment. Invariant and highly conserved amino acids are highlighted tangerine and blue, respectively. Residues involved in the interactions with Na^+ and Cl^- are labeled above the hTauT sequence.

The residues that form disulfide bonds are denoted by brown triangles.

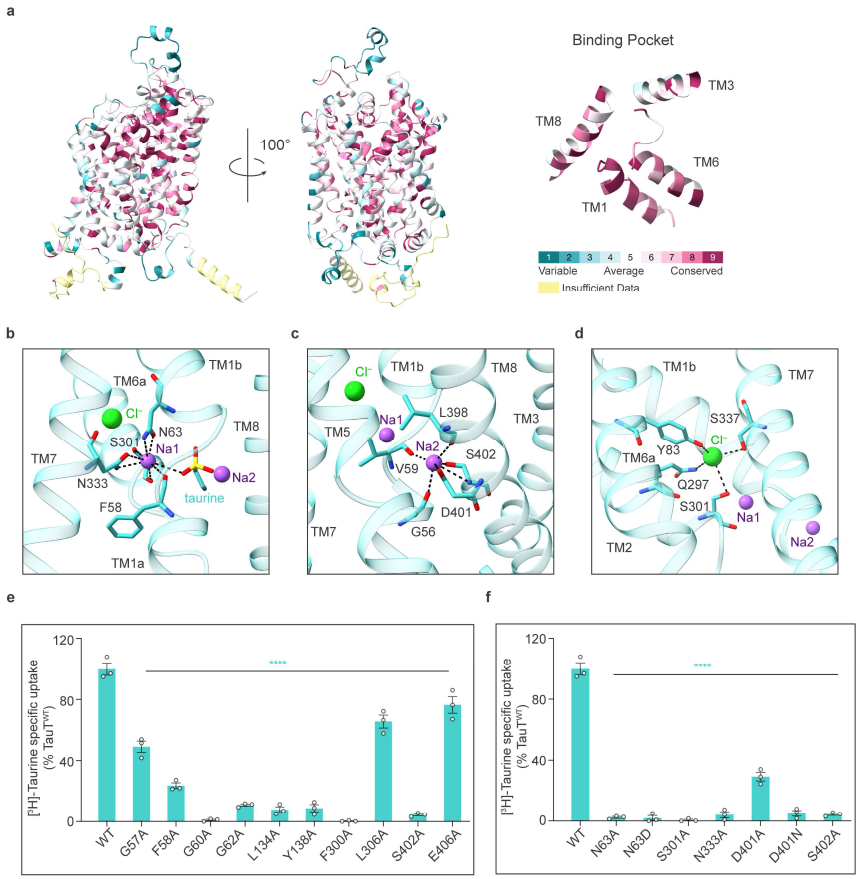

Supplementary Fig. 5 | Sequence conservation, ion recognition of hTauT and transport activity of TauT^{WT} and its mutants. (a) Sequence conservation analysis of hTauT in cartoon representation. Conservation is coloured as indicated. The binding pocket is highly conserved, with higher numbers denoting higher conservation. (**b-d)** Zoomed-in view of the binding pocket and interactions of the ions, namely Na1 **(b)**, Na2 **(c)** and Cl^- **(d)**. **(e-f)** Biochemical validation of the taurine **(e)** or ions **(f)** binding residues using [^{3}H]taurine uptake assay. The transport activity of each mutant is normalized to that of TauT^{WT}. Assays were conducted with three independent biological replicates (n=3). Data are mean ± s.e.m. Data were analysed by one-way ANOVA to show the significance compared with TauT^{WT}: ****P<0.0001. Source data are provided as a Source Data file.

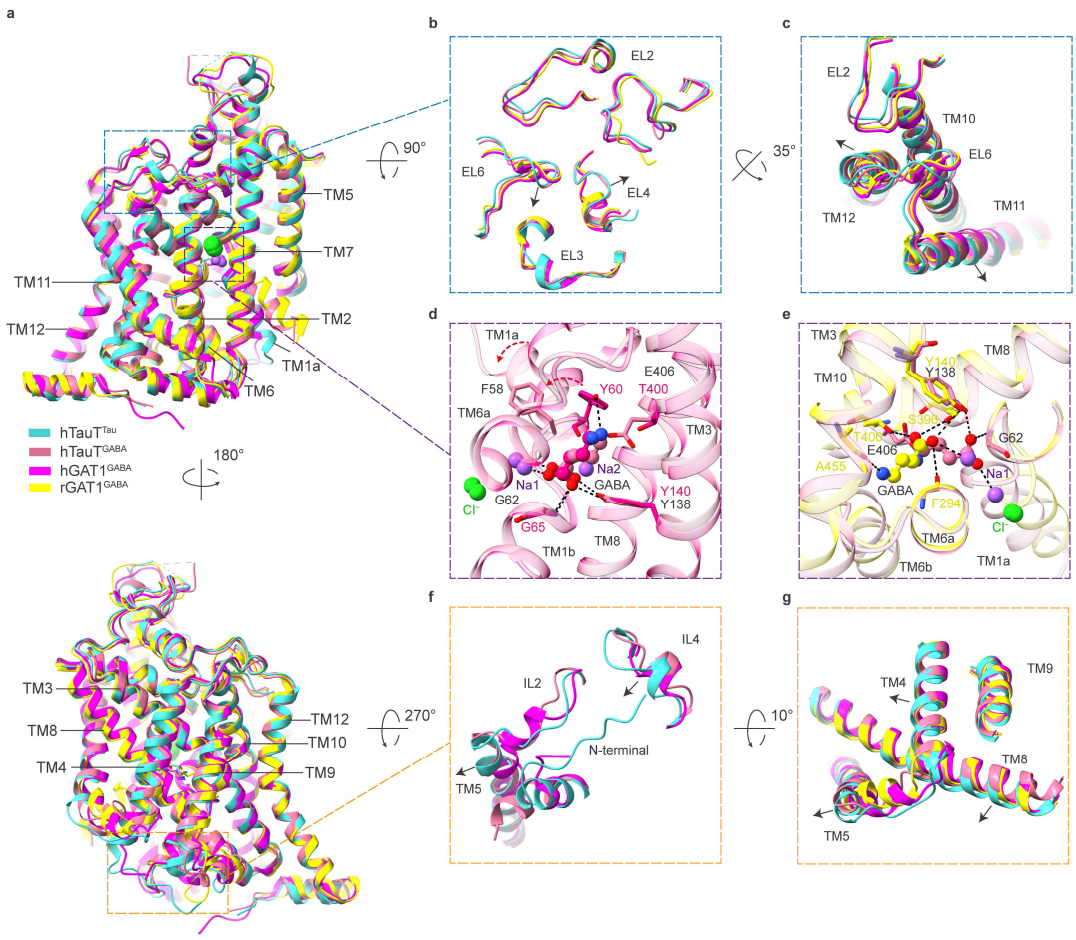

Supplementary Fig. 6 | Structural comparisons of hTauT, hGAT1 and rGAT1. (a) Structural comparisons of hTauT^{Tau}, hTauT^{GABA}, hGAT1^{GABA} (PDB:7Y7Y) and rGAT1^{GABA} (PDB:8GNK). The structures were superimposed onto hTauT. **(b)** Structural comparisons of ELs in hTauT, hGAT1 and rGAT1. **(c)** Structural comparisons of extracellular segments of TMs 10-12 in hTauT, hGAT1 and rGAT1. The directional movements of TMs 11-12 in hTauT relative to that in hGAT1 and rGAT1 are indicated by ash black arrows. **(d)** Superposition of the GABA binding sites of hTauT^{GABA} and hGAT1^{GABA} (PDB:7Y7Y). Key residues involved in GABA binding are visualized as sticks. GABAs are shown as light pink and dark pink in hTauT^{GABA} and hGAT1^{GABA}, respectively. **(e)** A comparative binding analysis between hTauT^{GABA} and rGAT1^{GABA}, highlighting their differences of binding positions. Structures of hTauT^{GABA} and rGAT1^{GABA} are colored light pink and yellow, respectively. **(f)** Structural comparisons of ILs in hTauT and hGAT1. The disrupted IL2 of hTauT causes TM5 to move outward. **(g)** Structural comparisons of TMs 4, 5, 8 and 9 in hTauT, hGAT1 and rGAT1. The directional movements are indicated by ash black arrows.

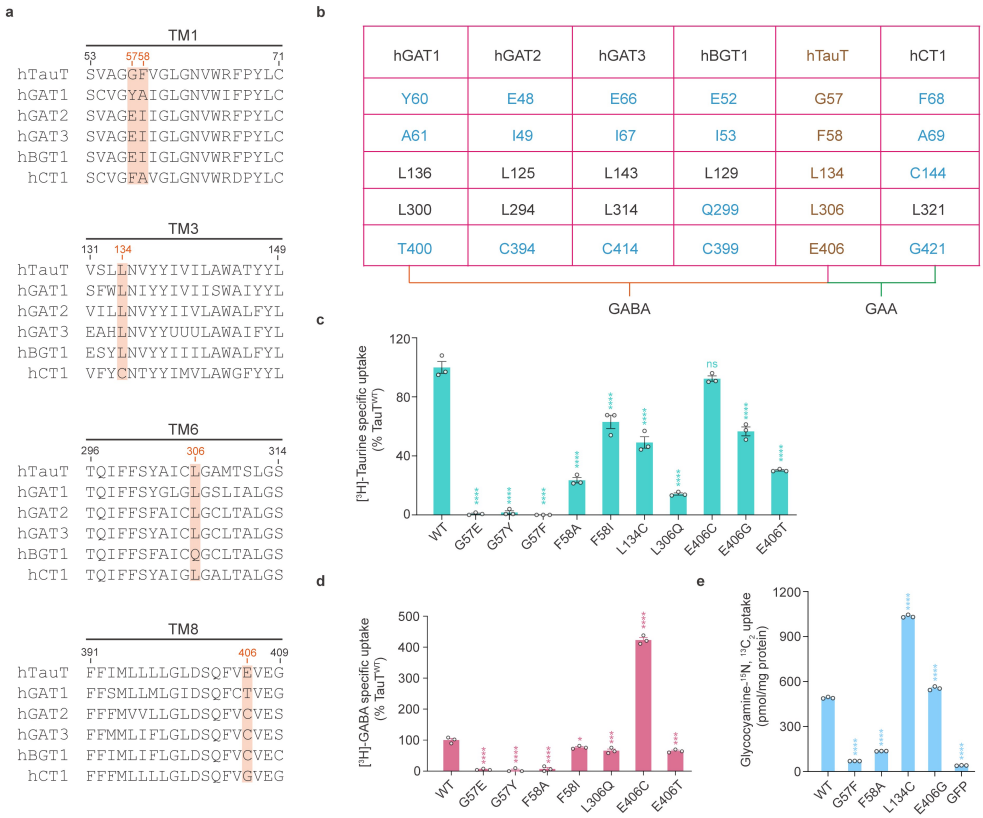

Supplementary Fig. 7 | Substrate specificity for GABA subfamily. (a-b) Sequence alignment of hTauT, hGATs, hBGT1 and hCT1. The numbers refer to position in the hTauT sequence. Residues non-conserved in the central binding pocket among hTauT, hGATs and hCT1 are boxed in orange **(a)** and are highlighted in blue **(b)**. **(c-e)** Effects of mutations on the transport activity of taurine **(c),** GABA **(d)** and GAA **(e)**. Data were generated and graphed as mean ± s.e.m. of three independent biological replicates (*n*=3). The transport activity of taurine and GABA of each mutant is normalized to that of $TauT^{WT}$. Data were analysed by one-way ANOVA to show the significance compared with $TauT^{WT}$: ****P<0.00001, ***P<0.0001, **P<0.001, *P<0.01. Source data are provided as a Source Data file.

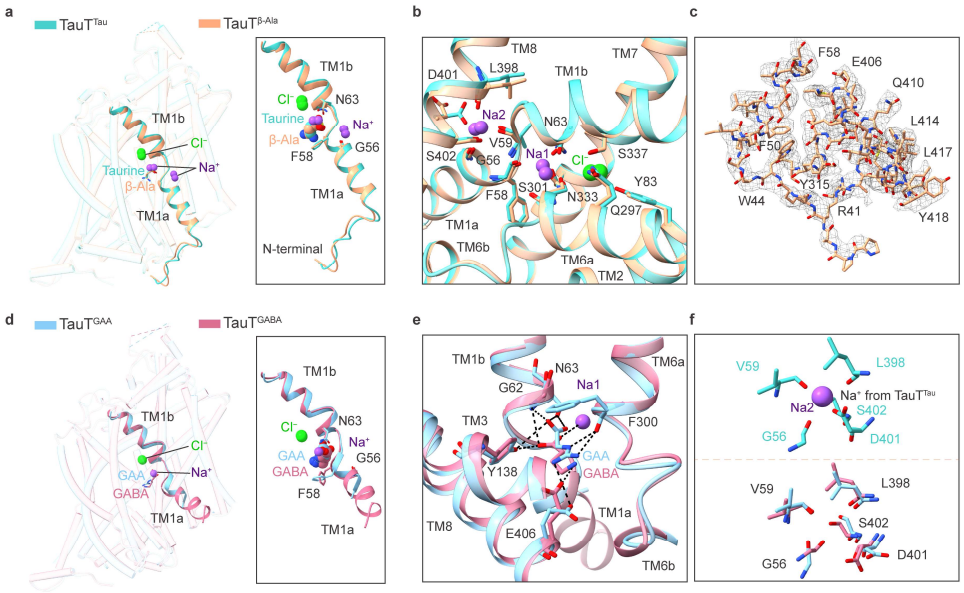

Supplementary Fig. 8 | Structural comparisons of TauT^{Tau}, TauT$^{β\text{-}Ala}$, TauT^{GAA} and TauT^{GABA}. (a) Structural comparisons between TauT^{Tau} (cyan) and TauT$^{β\text{-}Ala}$ (orange) in occluded states. TM1 of TauT^{Tau} and TauT$^{β\text{-}Ala}$ are depicted as cartoons, while other transmembrane helices are shown as cylinders. The taurine and β-Ala are shown as sticks. Na^+ and Cl^- are depicted as purple and green spheres, respectively. **(b)** Analysis of Na1, Na2, and Cl^- coordination in TauT^{Tau} and TauT$^{β\text{-}Ala}$. The key residues for interaction are presented as sticks and labeled. **(c)** Detailed view of the N-terminus of TauT$^{β\text{-}Ala}$. The electron density is depicted as a gray mesh and contoured at 5 σ by ChimeraX. Residues within the N-terminus are visualized as sticks. **(d)** Structural comparisons between TauT^{GAA} (blue) and TauT^{GABA} (pink) in an intermediate state. TM1 of TauT^{GAA} and TauT^{GABA} are depicted as cartoons, while other transmembrane helices are shown as cylinders. The GAA and GABA are shown as sticks. Na^+ and Cl^- are depicted as purple and green spheres, respectively. **(e)** Superposition of the ligand binding sites of TauT^{GAA} and TauT^{GABA}. Key residues involved in binding are visualized as sticks. **(f)** Expanded comparison view of the binding sites of Na2 between TauT^{GAA} and TauT^{GABA}.

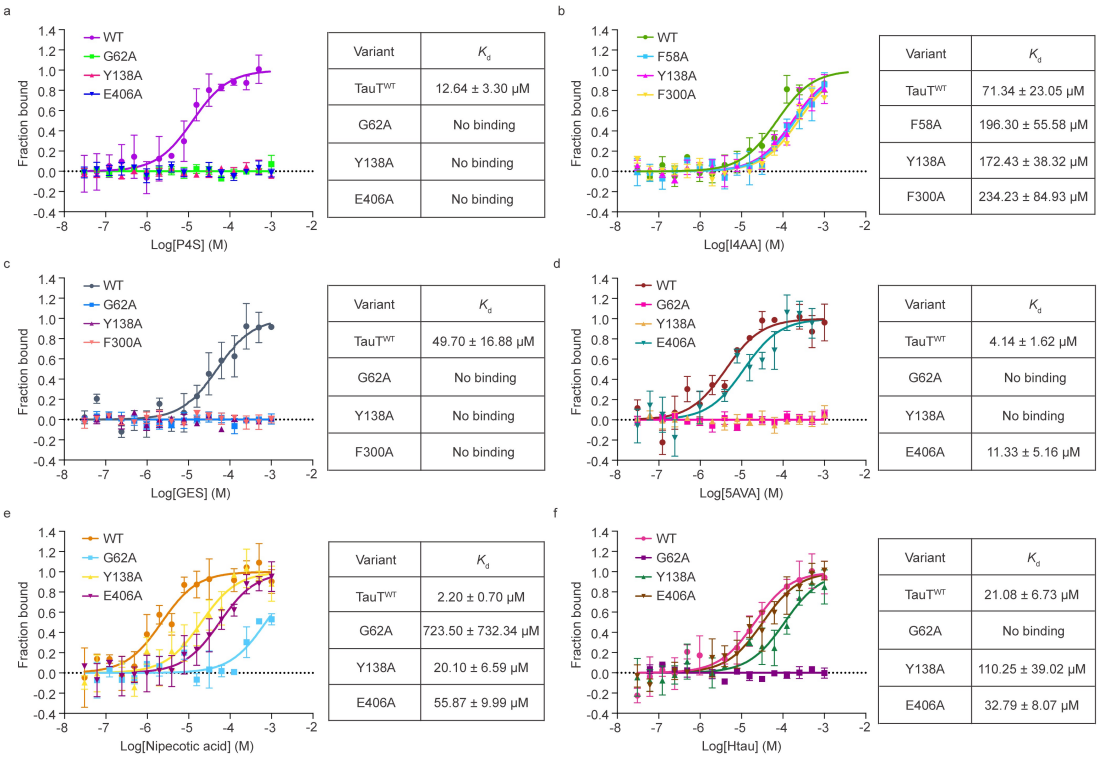

Variant	K_d
TauT^{WT}	12.64 ± 3.30 μM
G62A	No binding
Y138A	No binding
E406A	No binding

Variant	K_d
TauT^{WT}	71.34 ± 23.05 μM
F58A	196.30 ± 55.58 μM
Y138A	172.43 ± 38.32 μM
F300A	234.23 ± 84.93 μM

Variant	K_d
TauT^{WT}	49.70 ± 16.88 μM
G62A	No binding
Y138A	No binding
F300A	No binding

Variant	K_d
TauT^{WT}	4.14 ± 1.62 μM
G62A	No binding
Y138A	No binding
E406A	11.33 ± 5.16 μM

Variant	K_d
TauT^{WT}	2.20 ± 0.70 μM
G62A	723.50 ± 732.34 μM
Y138A	20.10 ± 6.59 μM
E406A	55.87 ± 9.99 μM

Variant	K_d
TauT^{WT}	21.08 ± 6.73 μM
G62A	No binding
Y138A	110.25 ± 39.02 μM
E406A	32.79 ± 8.07 μM

Supplementary Fig. 9 | Binding affinities for TauT mutants with six small molecular compounds measured using MST assay. (a-f) Left, microscale thermophoresis curves of P4S **(a)**, I4AA **(b)**, GES **(c)**, 5AVA **(d)**, nipecotic acid **(e)**, and Htau **(f)** binding to TauT and mutants. The curves were fitted using the data of three independent experiments. Right, the tables summarize the K_d values. Data are shown as mean ± s.e.m. K_d values are presented in μM. Assays were conducted with three independent biological replicates (n=3). Source data are provided as a Source Data file.

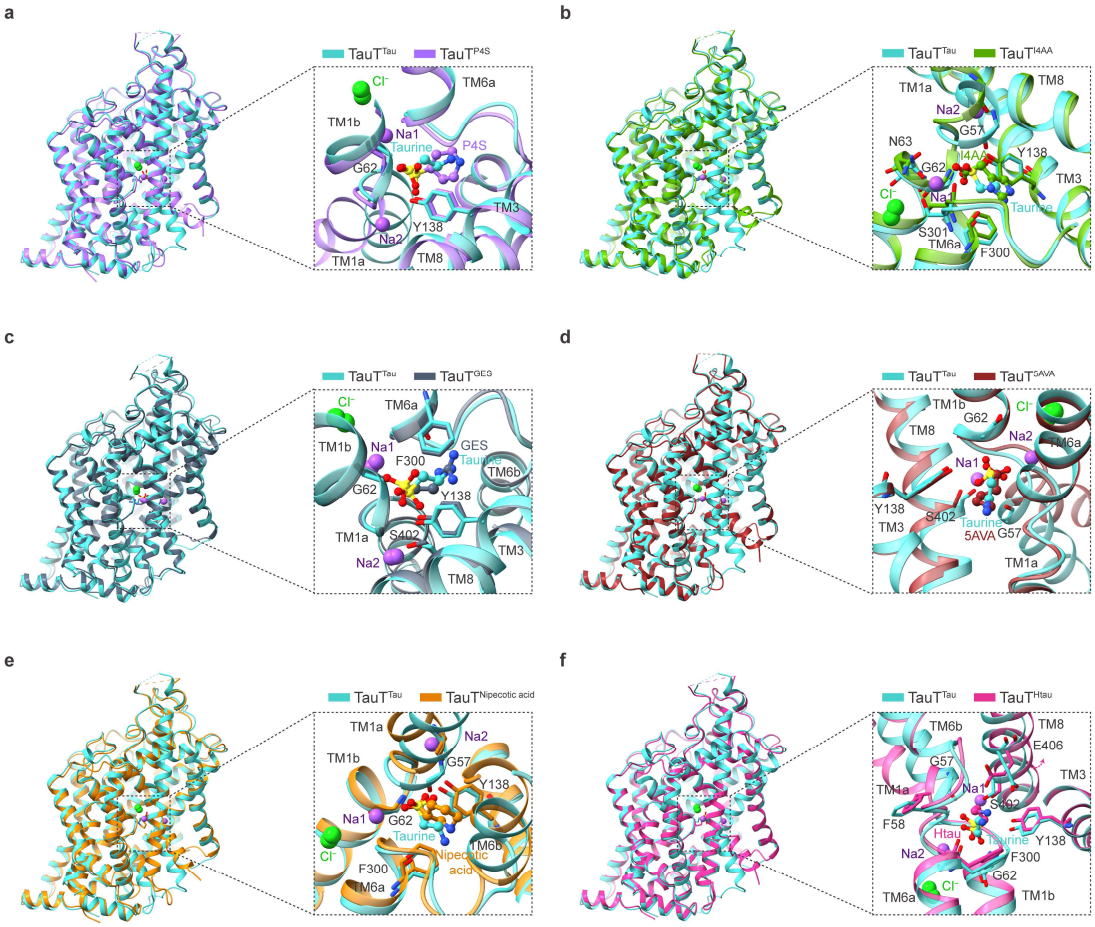

Supplementary Fig. 10 | Mechanisms of hTauT inhibition by small molecule compounds. (a-f) Structural comparisons of $TauT^{Tau}$ with $TauT^{P4S}$ **(a),** $TauT^{I4AA}$ **(b),** $TauT^{GES}$ **(c),** $TauT^{5AVA}$ **(d),** $TauT^{Nipecotic\ acid}$ **(e)** and $TauT^{Htau}$ **(f)**. Key residues involved in taurine and small molecule compounds binding are visualized as sticks and labeled. Small molecule compounds P4S, I4AA, GES, 5AVA, nipecotic acid and Htau are represented by purple, green, grayish blue, brick red, orange and deep pink ball sticks, respectively.

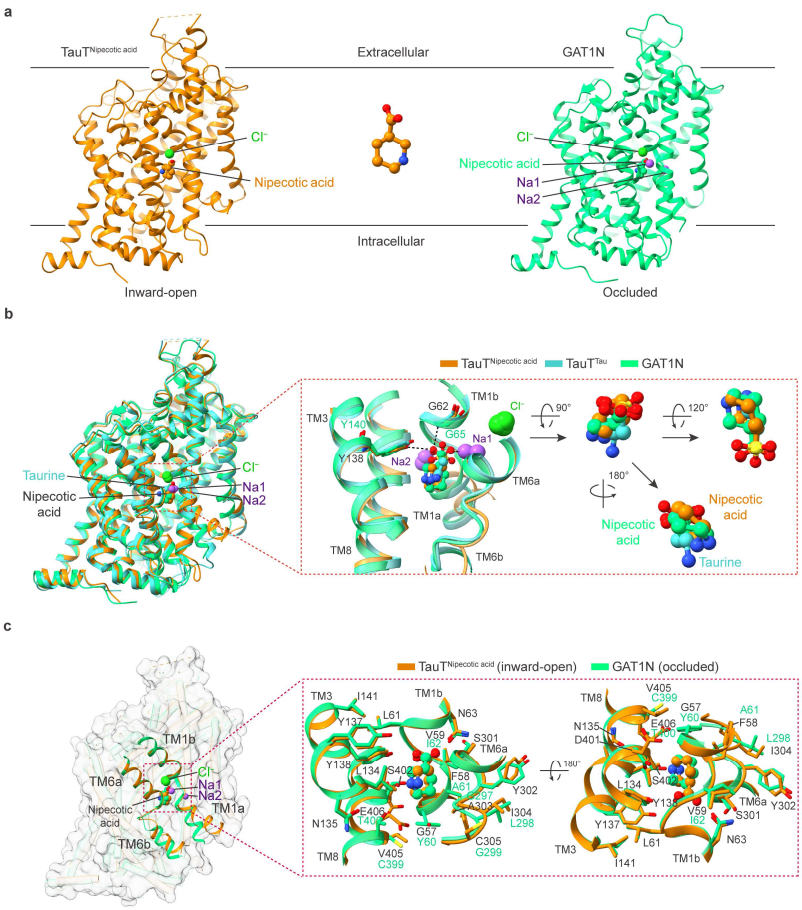

Supplementary Fig. 11 | Structural analysis of the nipecotic acid-bound hTauT and hGAT1. (a) Overall structural comparison between TauT$^{\text{Nipecotic acid}}$ in inward-open state (orange) and GAT1N (PDB: 7Y7W) in occluded state (green). TMs are depicted as cartoons. Nipecotic acid is displayed by spheres and labeled. Cl^- and Na^+ are colored as green and purple spheres, respectively. **(b)** Left, shown here are superimposed structures of TauT$^{\text{Tau}}$, TauT$^{\text{Nipecotic acid}}$ and GAT1N. Right, the nipecotic acid exhibit the same interaction pattern within the central binding pocket. Nipecotic acid aligns closely with taurine. **(c)** Left, structural superposition of TauT$^{\text{Nipecotic acid}}$ and GAT1N, among all the TMs, the major distinction occurs in TM1 and TM6. Nipecotic acid is depicted as ball stick. The surface of TauT$^{\text{Nipecotic acid}}$ is colored in gray. Right, comparison of the binding pocket of nipecotic acid in hTauT and hGAT1. Key residues forming the binding pocket are shown as sticks.

Supplementary Table 1. Cryo-EM data collection, refinement and validation statistics

	#1 $TauT^{Tau}$ (EMDB-61970) (PDB 9K1B)	#2 $TauT^{Apo}$ (EMDB-61943) (PDB 9K0C)	#3 $TauT^{\beta\text{-}Ala}$ (EMDB-61948) (PDB 9K0N)	#4 $TauT^{GAA}$ (EMDB-61949) (PDB 9K0O)	#5 $TauT^{GABA}$ (EMDB-61974) (PDB 9K1F)	#6 $TauT^{P4S}$ (EMDB-61975) (PDB 9K1H)
Data collection and processing						
Magnification	81,000 ×	81,000 ×	81,000 ×	81,000 ×	81,000 ×	81,000 ×
Voltage (kV)	300	300	300	300	300	300
Electron exposure (e–/Å^2)	50	50	50	50	50	50
Defocus range (μm)	−1.0~−2.0	−1.0~−2.0	−1.0~−2.0	−1.0~−2.0	−1.0~−2.0	−1.0~−2.0
Pixel size (Å)	1.095	1.072	1.072	1.072	1.072	1.072
Symmetry imposed	C1	C1	C1	C1	C1	C1
Initial particle images (no.)	5,386,531	3,943,377	8,316,520	5,067,322	4,279,971	13,585,527
Final particle images (no.)	192,228	828,600	631,153	312,753	250,445	587,727
Map resolution (Å)	3.34	3.06	3.21	2.95	3.43	3.12
FSC threshold	0.143	0.143	0.143	0.143	0.143	0.143
Map resolution range (Å)	2.7-3.5	2.5-3.3	2.5-3.3	2.4-3.2	2.8-3.6	2.5-3.3
Refinement						
Initial model used (PDB code)			AlphaFold-P31641			
Model resolution (Å)	3.48	3.17	3.33	3.16	3.56	3.24
FSC threshold	0.5	0.5	0.5	0.5	0.5	0.5
Model resolution range (Å)	NA	NA	NA	NA	NA	NA
Map sharpening *B* factor (Å^2)	-117.4	-138.6	-155.4	-108.5	-128.4	-133.7
Model composition						
Non-hydrogen atoms	5617	5589	5664	5535	5588	5596
Protein residues	763	754	763	746	754	754
Ligands	1	None	1	1	1	1
ions	Na^+: 2, Cl^-: 1	Cl^-: 1	Na^+: 2, Cl^-: 1	Cl^-: 1	Na^+: 1, Cl^-: 1	Cl^-: 1
B factors (Å^2)						
Protein	43.86	48.71	67.75	39.66	43.98	40.89
Ligand	34.03	79.69	88.41	102.46	56.79	61.94
R.m.s. deviations						
Bond lengths (Å)	0.007	0.004	0.004	0.006	0.005	0.005
Bond angles (°)	1.055	1.012	0.920	1.102	1.027	1.069
Validation						
MolProbity score	1.38	1.22	1.34	1.27	1.30	1.49
Clash score	4.42	3.97	4.37	3.08	4.62	6.26
Rotamer outliers (%)	0.37	0.55	0.00	0.93	0.37	0.37
Ramachandran plot						
Favored (%)	97.09	97.86	97.35	97.02	97.72	97.18
Allowed (%)	2.91	2.14	2.65	2.98	2.28	2.82
Disallowed (%)	0.00	0.00	0.00	0.00	0.00	0.00

Continued Supplementary Table 1.

	#7 TauT^{I4AA} (EMDB-61976) (PDB 9K1I)	#8 TauT^{GES} (EMDB-61983) (PDB 9K1X)	#9 TauT^{5AVA} (EMDB-61983) (PDB 9K1V)	#10 TauT^{Htau} (EMDB-61987) (PDB 9K21)	#11 TauT$^{Nipecotic\ acid}$ (EMDB-61985) (PDB 9K1Z)
Data collection and processing					
Magnification	81,000 ×	81,000 ×	81,000 ×	81,000 ×	81,000 ×
Voltage (kV)	300	300	300	300	300
Electron exposure (e–/Å^2)	50	50	50	50	50
Defocus range (μm)	−1.0~−2.0	−1.0~−2.0	−1.0~−2.0	−1.0~−2.0	−1.0~−2.0
Pixel size (Å)	1.072	1.072	1.072	1.072	1.072
Symmetry imposed	C1	C1	C1	C1	C1
Initial particle images (no.)	13,949,419	3,610,081	5,065,063	4,506,467	6,115,247
Final particle images (no.)	696,736	254,623	451,715	164,725	299,041
Map resolution (Å)	2.92	3.06	2.94	3.45	3.27
FSC threshold	0.143	0.143	0.143	0.143	0.143
Map resolution range (Å)	2.3-3.1	2.6-3.4	2.3-3.1	2.8-3.6	2.5-3.3
Refinement					
Initial model used (PDB code)			AlphaFold-P31641		
Model resolution (Å)	3.05	3.19	3.09	3.58	3.42
FSC threshold	0.5	0.5	0.5	0.5	0.5
Model resolution range (Å)	NA	NA	NA	NA	NA
Map sharpening *B* factor (Å^2)	-120.0	-112.4	-111.4	-124.9	-121.0
Model composition					
Non-hydrogen atoms	5608	5569	5592	5492	5531
Protein residues	754	754	754	754	754
Ligands	1	1	1	1	1
ions	Cl^-: 1	Na^+: 2, Cl^-: 1	Cl^-: 1	Cl^-: 1	Cl^-: 1
B factors (Å^2)					
Protein	42.34	57.87	35.46	82.08	58.58
Ligand	46.61	59.15	72.46	38.48	21.61
R.m.s. deviations					
Bond lengths (Å)	0.006	0.006	0.004	0.007	0.006
Bond angles (°)	1.128	1.060	0.976	1.184	1.036
Validation					
MolProbity score	1.47	1.49	1.42	1.35	1.32
Clash score	4.98	4.27	6.01	4.47	4.87
Rotamer outliers (%)	1.29	1.50	1.29	0.00	0.19
Ramachandran plot					
Favored (%)	97.32	97.18	97.99	97.32	97.72
Allowed (%)	2.68	2.82	2.01	2.68	2.28
Disallowed (%)	0.00	0.00	0.00	0.00	0.00

Supplementary Table 2. Effects of mutations on the binding affinity for substrate and substrate analogues. The binding affinity was measured using MST assay treated with different concentrations of ligands. Data shown are means ± s.e.m of three independent biological replicates (n=3). K_d values are presented in μM.

Variants	Ligands			
	Taurine	β-Ala	GAA	GABA
$TauT^{WT}$	0.71 ± 0.13 μM	0.72 ± 0.28 μM	35.81 ± 16.00 μM	26.03 ± 12.55 μM
F58A	16.75 ±4.72 μM	41.76 ± 14.83 μM		
G62A			No binding	No binding
Y138A	No binding	No binding	No binding	No binding
F300A	656.82 ± 803.56 μM	No binding	No binding	No binding
L306A			No binding	740.03 ± 1071.7 μM
S402A	No binding	871.65 ±1469.9 μM		
E406A	25.77 ± 6.33 μM	No binding	58.95 ± 20.14 μM	138.73 ± 43.08 μM